Attenuation of surface acoustic phonons in metallic superlattices

2003 J. Phys.: Condens. Matter 15 693

(http://iopscience.iop.org/0953-8984/15/4/309)

INSTITUTE OF PHYSICS PUBLISHING JOURNAL OF PHYSICS: CONDENSED MATTER

J. Phys.: Condens. Matter **15** (2003) 693–707 PII: S0953-8984(03)39318-X

Attenuation of surface acoustic phonons in metallic superlattices

N Perrin[1] **and S Tamura**[2]

[1] Laboratoire de Physique de la Matière Condensée de l'Ecole Normale Superieure, 24 rue Lhomond, 75231 Paris Cedex 5, France
[2] Department of Applied Physics, Hokkaido University, Sapporo 060-8628, Japan

Received 10 July 2002
Published 20 January 2003
Online at stacks.iop.org/JPhysCM/15/693

Abstract

We consider the interaction of the acoustic phonons localized at the free surface (surface phonons) in semi-infinite metallic superlattices with electrons and the resulting surface phonon attenuation rates. We assume a semi-infinite Kronig–Penney model for the electrons, and the acoustic surface phonons in the superlattices are described through the continuum elasticity theory. The deformation-potential coupling is used to calculate the attenuation rates of the surface phonons in the superlattice. The results are compared with the experimental damping rates of the localized vibrational modes at the surface of Al/Ag superlattices.

1. Introduction

The existence of acoustic waves localized at solid surfaces has been well known since the earlier study by Lord Rayleigh [1]. Recently, a considerable number of studies have been made on the surface acoustic waves in multilayered elastic systems, or superlattices [2–8]. These surface vibrations may appear within the extra gaps that exist between the folded bulk bands [9, 10]. They depend on the kind of layer near the surface [5]; they have been predicted to exist when the surface layer has smaller acoustic impedance [2, 6, 11, 12].

Surface vibrations have been observed experimentally in both semiconducting and metallic superlattices: first by Grahn *et al* [11] in Si/Ge, then by Chen *et al* [12] in Al/Ag and by Perrin *et al* [13] in Cu/W superlattices. Specifically, with the picosecond ultrasonics based on a pump–probe optical technique, Chen *et al* [12] observed the longitudinal lattice vibrations that remain near to the free surface for longer than 200 ps. This has been seen with an aluminium surface layer but no such persistent oscillation has been observed with a silver surface layer. Here we may point out that the acoustic impedance Z_{Al} of aluminium for the longitudinal mode is smaller than the corresponding acoustic impedance Z_{Ag} of silver ($Z_{\mathrm{Al}} = 1.73 \times 10^6$ g cm^{-2} s^{-1} $< Z_{\mathrm{Ag}} = 4.2 \times 10^6$ g cm^{-2} s^{-1}).

The frequencies of the observed surface vibrations are in good agreement with the values predicted in the scope of the elasticity theory [12], but their damping is not so simple. The

measured attenuation rate of the surface vibrations at the mini-Brillouin zone boundary varies linearly with frequency, in the range 100–300 GHz for various bilayer thicknesses. This linear variation of the attenuation with frequency may be a signature of an electron–phonon interaction as in the Pippard theory in bulk metals [14]. However, the agreement between the measured attenuation rate and the expected values from Pippard theory is far from being perfect; the measured attenuation is larger than the values expected for bulk aluminium and bulk silver with ratios of three and 25, respectively. Since the attenuation rate of bulk phonons in Al is about one order of magnitude larger than the attenuation rate in Ag, the superlattice samples containing thicker Al layers may be thought to exhibit a larger damping. This has not, however, been observed in the experiments by Chen *et al* with different ratios of the Al to Ag thicknesses. Accordingly, they have attributed the observed attenuation to interaction of nonelectronic origin [12].

The purpose of the present work is to study quantitatively the effects of the folded band structures on the attenuation of surface phonons in metallic superlattices in order to compare to the attenuation for phonons in bulk metals. In a previous paper [15], we have studied the correction to the Pippard theory of the attenuation of bulk longitudinal acoustic phonons in a perfect periodic superlattice; we have predicted a remarkable feature, i.e. the resonant absorption of the phonons by the electrons due to the Brillouin-zone folding of the electrons. This effect never happens in a homogeneous elastic space.

Theoretically the surface phonons localized at the truncated surface of a semi-infinite superlattice are obtained by solving the equations of motion for the lattice displacement under the stress-free boundary condition at the surface and their frequencies are found inside bandgaps of the corresponding perfect, periodic superlattice. For the electrons we assume a semi-infinite Kronig–Penney model. The deformation potential coupling is used for the electron–acoustic phonon interaction as assumed in [15].

In section 2 we summarize the formulation of surface phonons in semi-infinite superlattices with a free surface and give explicit expressions for the acoustic displacement fields associated with the surface modes. The electron fields in the semi-infinite Kronig–Penney model are given in section 3 and the electron–phonon interaction is formulated in section 4. The expressions for the resulting scattering rates of the surface phonons and the corresponding numerical calculations for Al/Ag superlattices are developed respectively in sections 5 and 6. Discussion and concluding remarks are given in section 7.

2. Surface phonons in a semi-infinite superlattice with a free surface

The periodic superlattice considered here consists of alternating A and B layers of elastically isotropic materials with layer thicknesses d_A and d_B, densities ρ_A and ρ_B and sound velocities v_A and v_B, respectively. The unit period, or bilayer thickness, is $D = d_A + d_B$. The layer interfaces of the superlattice are taken to be parallel to the $\boldsymbol{x}_\parallel = (x, y)$ plane and the growth direction is parallel to the z direction. We study the surface vibrations (surface phonons) whose displacement amplitudes decay in the z direction perpendicular to the layer interfaces. As observed in the experiments by Chen *et al* [12], here we assume that these surface phonons do not propagate in the direction along the layer interfaces, i.e., $\boldsymbol{k}_\parallel = 0$, where $\boldsymbol{k}_\parallel$ is the two-dimensional wavevector in the $\boldsymbol{x}_\parallel$ plane. For $\boldsymbol{k}_\parallel = 0$, the three vibrational modes are decoupled from each other and we consider a single mode. The surface wave solutions are obtained by solving the equations of motion for the lattice displacement under the stress-free boundary condition at the surface. The continuity of the lattice displacement and stress at the interface between any two layers leads to a 2×2 transfer matrix T [4, 6, 12, 15] as defined below: the general solution for the longitudinal lattice displacement is written in the

form $\boldsymbol{w}(z) = (0, 0, W(z))$ and the time-dependent lattice displacement in the direction z is $u(z, t) = W(z) \exp(-\mathrm{i}\omega t)$, with ω an angular frequency. Within the theory of elasticity and in the above conditions, the lattice displacement u is related to the zz component σ of the elastic stress tensor by [15]

$$\sigma(z, t) = \rho v^2 \partial u/\partial z, \tag{1}$$

where $\partial u/\partial z$ is the strain. The mass density ρ (the sound velocity v) takes either the value $\rho_{\mathrm{A}}(v_{\mathrm{A}})$ or $\rho_{\mathrm{B}}(v_{\mathrm{B}})$ depending on the layer considered. The lattice displacement $u(z, t)$ and the stress σ satisfy the equation of motion

$$\rho \frac{\partial^2 u(z, t)}{\partial t^2} = \frac{\partial \sigma(z, t)}{\partial z}. \tag{2}$$

In the superlattices with bilayer thickness larger than about 100 Å, the use of the continuum model with bulk values for the sound velocities and mass densities uniform in each layer should be valid.

Previously, we have used the transfer-matrix method to study the propagating bulk phonons and their attenuation in metallic superlattices [15]. In that work it was shown that the matrix elements of the unimodular matrix T satisfying $\det T = 1$ are functions of $k_{\mathrm{A}}, d_{\mathrm{A}}, k_{\mathrm{B}}, d_{\mathrm{B}}$, Z_{A} and Z_{B}, where $k_I = \omega/v_I$ $(I = A, B)$ is the wavenumber in each constituent layer and $Z_I = \rho_I v_I$ is the acoustic impedance [2–6, 11, 12, 16]. We recall here the matrix elements of T:

$$T_{11} = \cos(k_{\mathrm{A}} d_{\mathrm{A}}) \cos(k_{\mathrm{B}} d_{\mathrm{B}}) - \frac{Z_{\mathrm{A}}}{Z_{\mathrm{B}}} \sin(k_{\mathrm{A}} d_{\mathrm{A}}) \sin(k_{\mathrm{B}} d_{\mathrm{B}}), \tag{3}$$

$$T_{12} = Z_{\mathrm{A}}^{-1} \sin(k_{\mathrm{A}} d_{\mathrm{A}}) \cos(k_{\mathrm{B}} d_{\mathrm{B}}) + Z_{\mathrm{B}}^{-1} \cos(k_{\mathrm{A}} d_{\mathrm{A}}) \sin(k_{\mathrm{B}} d_{\mathrm{B}}), \tag{4}$$

$$T_{21} = -Z_{\mathrm{A}} \sin(k_{\mathrm{A}} d_{\mathrm{A}}) \cos(k_{\mathrm{B}} d_{\mathrm{B}}) - Z_{\mathrm{B}} \cos(k_{\mathrm{A}} d_{\mathrm{A}}) \sin(k_{\mathrm{B}} d_{\mathrm{B}}), \tag{5}$$

$$T_{22} = \cos(k_{\mathrm{A}} d_{\mathrm{A}}) \cos(k_{\mathrm{B}} d_{\mathrm{B}}) - \frac{Z_{\mathrm{B}}}{Z_{\mathrm{A}}} \sin(k_{\mathrm{A}} d_{\mathrm{A}}) \sin(k_{\mathrm{B}} d_{\mathrm{B}}). \tag{6}$$

In a semi-infinite superlattice with a free surface, the perfect periodicity of the system is lost and the Bloch theorem no longer applies. A boundary condition is now introduced: the stress must vanish at the free surface. This boundary condition at the surface leads to the condition $T_{21} = 0$ for the transfer matrix and the possible existence of acoustic modes that are localized near the surface of the semi-infinite superlattice. The theory of such surface modes has so far been extensively discussed [2, 4–6]. The above condition together with the equation $\det(T) = 1$ leads to the dispersion relation of these non-propagating modes with $\boldsymbol{k}_{\parallel} = 0$ as $\cos(k_z D) = \mathrm{tr}(T)/2 = (T_{11} + T_{22})/2 \geqslant 1$ [6, 11, 12], where $\exp(\mathrm{i}k_z D)$ is an eigenvalue of the transfer matrix T. The superlattice wavenumber k_z governing the wave motion in the z direction is complex and the surface phonon frequencies $\omega = \omega_\ell$ $(\ell = 1, 2, \ldots)$ are found inside the bandgaps of a perfect, periodic superlattice [15].

The ratio of the lattice displacements at the two adjacent periods of the superlattice is T_{11} if the equation $T_{12} = 0$ is satisfied [6] and the corresponding expression of T_{11} is deduced from equations (3) and (4). Since surface modes must decay exponentially as one travels away from the surface, T_{11} must satisfy the condition $|(T_\ell)_{11}| \equiv |[T(\omega_\ell)]_{11}| < 1$ [6]. Therefore among the above possible frequencies only those satisfying

$$|(T_\ell)_{11}| = \left| \frac{\cos\left(\frac{\omega_\ell d_{\mathrm{A}}}{v_{\mathrm{A}}}\right)}{\cos\left(\frac{\omega_\ell d_{\mathrm{B}}}{v_{\mathrm{B}}}\right)} \right| < 1 \tag{7}$$

correspond to the frequencies of the vibrational modes localized near the surface [6, 11, 12]. Such eigenfrequencies have been obtained by Chen *et al* for an Al/Ag superlattice (see figure 1) with $d_{\mathrm{B}}/d_{\mathrm{A}} = 0.8$, $D = d_{\mathrm{A}} + d_{\mathrm{B}} = 218$ Å and an Al surface layer A = Al [12]. The decay

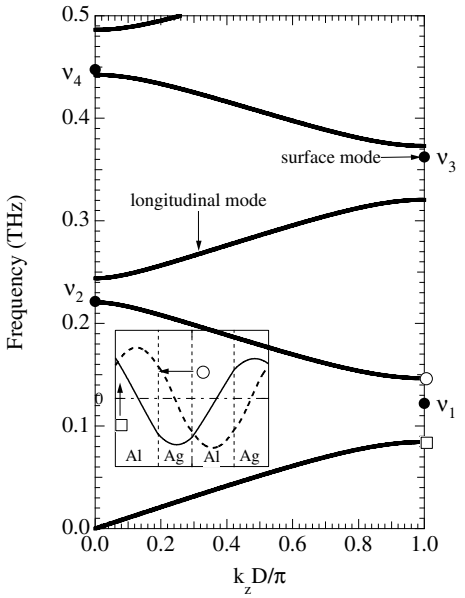

Figure 1. The eigenfrequencies of the surface modes in the semi-infinite Al/Ag superlattice with an Al (A) layer at the surface are represented by the dots at $k_z D/\pi = 0$ and 1. The dispersion relations of longitudinal phonons propagating normal to the layer interfaces of the superlattice are also shown (solid curves) with $d_A = d_{Al} = 121$ Å and $d_B = d_{Ag} = 97$ Å ($D = d_A + d_B = 218$ Å). The lattice displacement equation (9) in the superlattice at the lower edge (solid curve) and the upper edge (dashed curve) of the lowest frequency gap is shown in the inset with the open square and circle, respectively.

profiles of the lattice displacements for the lowest two surface mode frequencies are shown in figure 2. The surface acoustic modes have also been studied by several groups either for transverse modes [2], or sagittal modes [4].

From the above considerations, the quantized surface phonon displacement vector $\boldsymbol{u}$ for $\boldsymbol{k}_\parallel = 0$ in the semi-infinite superlattices can be written as

$$\boldsymbol{u}(\boldsymbol{x}) = \sum_J \left(\frac{\hbar}{2\omega_J S}\right)^{1/2} (a_J + a_{-J}^\dagger)\boldsymbol{w}_J(z), \tag{8}$$

where $\boldsymbol{x} = (\boldsymbol{x}_\parallel, z)$, $J = \ell$ is the index specifying the eigenfrequency ω_ℓ for the surface phonons, S is the normalization area, a_J and its Hermitian conjugate $a_J^\dagger$ are the annihilation and creation operators of a surface phonon satisfying $[a_J, a_{J'}^\dagger] = \delta_{J,J'}$ and $\boldsymbol{w}_J(z) = (0, 0, W_J(z))$ for the mode considered in the present work. Explicitly, the lattice displacement $W_J(z)$ is written as

$$W_J(z) = \sum_n (\xi_J)^n \{\Theta(z - nD)\Theta(nD + d_A - z)\rho_A^{-1/2} U_{A,J}^{(n+1)}(z) + \Theta(z - nD - d_A)\Theta[(n+1)D - z]\rho_B^{-1/2} U_{B,J}^{(n+1)}(z)\}, \tag{9}$$

$$U_{A,J}^{(n+1)}(z) = \tilde{A}_{1,J} \cos[k_A(z - nD)] + \tilde{A}_{2,J} \sin[k_A(z - nD)], \tag{10}$$

$$U_{B,J}^{(n+1)}(z) = \tilde{B}_{1,J} \cos[k_B(z - nD - d_A)] + \tilde{B}_{2,J} \sin[k_B(z - nD - d_A)], \tag{11}$$

where $\Theta(z)$ is the Heaviside unit-step function ($\Theta(z) = 1$ for $z \geqslant 0$ and $\Theta(z) = 0$ for $z < 0$) and $\xi_J = (T_\ell)_{11}$ for the surface phonons. For the semi-infinite superlattice occupying

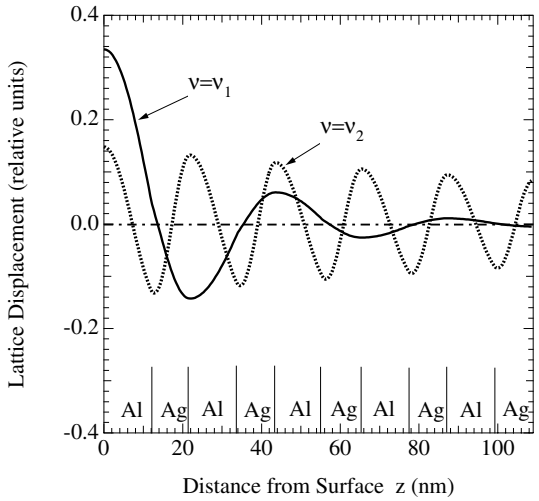

Figure 2. Lattice displacement $W_J(z)(J = \ell)$ versus distance z from the surface of the localized surface vibrations at the lowest two eigenfrequencies $\nu_\ell = \nu_1$ (solid curve) and $\nu_\ell = \nu_2$ (dotted curve) shown in figure 1.

$z > 0$ with the free surface located at $z = 0$ the summation over n extends from $n = 0$ to infinity where n specifies the position of the unit period considered. The coefficients $\tilde{A}_{m,J}$ and $\tilde{B}_{m,J}(m = 1, 2)$ in equations (10) and (11) are determined from the boundary conditions, i.e., the continuities of the lattice displacement W_J and the associated stress at layer interfaces, and also the normalization condition $\int_0^\infty \rho|W_J(z)|^2\,\mathrm{d}z = 1$, where ρ takes either the value ρ_A or ρ_B depending on the position z.

3. Electron field in a semi-infinite Kronig–Penney model

The intrinsic Fermi energies of the bulk metals constituting a periodic superlattice (e.g., Al and Ag to be studied) are different, in general. Therefore, at the metal–metal contacts a charge transfer should occur through each interface between two adjacent layers to achieve a uniform Fermi energy in the thermal equilibrium state. Also the charge neutrality should be satisfied locally, otherwise an electric field is set up which induces an electric current inside the system. As a result the potential for electrons $V(\boldsymbol{r}) = V(z)$ $(=V_I$ and I is either A or B depending on the position z in the system) is induced. We assume here that the transition between the values V_A and V_B of the potential occurs in a very narrow region at the interfaces. Therefore, in this abrupt interface approximation, we may assume a semi-infinite Kronig–Penney model [17] for the motion in the z direction perpendicular to the layer interfaces in the superlattice with a free surface at $z = 0$. Moreover, we assume a uniform mass in the layering structure with $m_\mathrm{A} = m_\mathrm{B} = m$, the free electron mass.

In contrast to the case of a perfect, periodic system, the momentum $\hbar p_z$ of an electron is not a good quantum number in the semi-infinite system. A significant effect induced by the introduction of the surface is the existence of surface localized states of electrons. This is similar to the case for phonons and the surface states appear inside the energy gaps of the original spectrum of electrons separated from the band edge states of the perfect, periodic system [18–20]. Along the layer interfaces the wavefunction should be described by a plane wave $\exp(\mathrm{i}\boldsymbol{p}_\parallel \cdot \boldsymbol{x}_\parallel)$ with $\boldsymbol{p}_\parallel$ the two-dimensional wavevector in the $\boldsymbol{x}_\parallel$-plane. Thus the total

wavefunction $\psi(\boldsymbol{r})$ is $\psi(\boldsymbol{r}) = \exp(\mathrm{i}\boldsymbol{p}_\parallel \cdot \boldsymbol{x}_\parallel)\phi_\lambda(z)$ and the wavefunction $\phi_\lambda(z)$ describing the electronic motion in the z direction satisfies the equation

$$\left[-\frac{\hbar^2}{2m}\frac{\mathrm{d}^2}{\mathrm{d}z^2} + V(z)\right]\phi_\lambda(z) = E_\lambda\phi_\lambda(z), \tag{12}$$

with the boundary conditions, i.e., the continuity of $\phi_\lambda(z)$ and of the component of its derivative normal to the interface $\partial\phi_\lambda(z)/\partial z$. The quantum number λ in the infinite Kronig–Penney model is expressed in terms of the Bloch wavenumber p_z and the band index i, i.e., $\lambda = (p_z, i)$, but in the semi-infinite Kronig–Penney model we express λ by a single index s, i.e., $\lambda = s$, which takes either discrete or continuous numbers corresponding to the surface and extended electronic states, respectively. Thus we write $\Lambda = (\boldsymbol{p}_\parallel, \lambda) = (\boldsymbol{p}_\parallel, s)$ and the total energy of an electron is $E_\Lambda = E_{\boldsymbol{p}_\parallel} + E_\lambda = E_{\boldsymbol{p}_\parallel} + E_s$. The continuous energy spectrum of the extended electrons in the semi-infinite superlattice is essentially the same as the one in the allowed energy band of the perfect, periodic superlattice [15]. This is because the energies of electrons of both the infinite (perfect, periodic) and semi-infinite periodic systems are determined from the eigenvalues of the same transfer matrix which connects the wavefunctions and their derivatives of adjacent periods and are insensitive to the boundary conditions [21, 22]. The energies giving the eigenvalues of unit modulus are inside the allowed band corresponding to real electron momentum p_z for the perfect, periodic Kronig–Penney model [15]. We will discuss this point in more detail in section 5.

We define here V_0 as the potential height of the barrier layer B for electrons relative to the well layer A for electrons, which results from the difference of the Fermi energies E_f^{A} and E_f^{B} of bulk A and B materials, i.e., $V_0 = E_f^{\mathrm{A}} - E_f^{\mathrm{B}} > 0$ (see figure 3). The envelope function $\phi_\lambda = \phi_s(z)$ for $z > 0$ takes a form similar to the expression of $W_J(z)$ for the phonons with a quantum number s instead of J [23],

$$\phi_s(z) = \sum_{n\geqslant 0}\{\Theta(z - nD)\Theta(nD + d_{\mathrm{A}} - z)\tilde{\phi}_{\mathrm{A},s}^{(n+1)}(z) + \Theta(z - nD - d_{\mathrm{A}})\Theta[(n+1)D - z]\tilde{\phi}_{\mathrm{B},s}^{(n+1)}(z)\}, \tag{13}$$

where $\tilde{\phi}_{\mathrm{A},s}^{(n+1)}(z)$ and $\tilde{\phi}_{\mathrm{B},s}^{(n+1)}(z)$ take similar forms as $U_{\mathrm{A},J}^{(n+1)}(z)$ and $U_{\mathrm{B},J}^{(n+1)}(z)$ for phonons given in equations (10) and (11). For the $(n+1)$th period and for $E_s > V_0$,

$$\tilde{\phi}_{\mathrm{A},s}^{(n+1)}(z) = A_{1,s}^{(n+1)}\cos[q_{\mathrm{A}}(z - nD)] + A_{2,s}^{(n+1)}\sin[q_{\mathrm{A}}(z - nD)], \tag{14}$$

$$\tilde{\phi}_{\mathrm{B},s}^{(n+1)}(z) = B_{1,s}^{(n+1)}\cos[q_{\mathrm{B}}(z - nD - d_{\mathrm{A}})] + B_{2,s}^{(n+1)}\sin[q_{\mathrm{B}}(z - nD - d_{\mathrm{A}})]. \tag{15}$$

The wavenumbers q_{A} and q_{B} are defined through the energy of electrons $E_s = \hbar^2 q_{\mathrm{A}}^2/2m = \hbar^2 q_{\mathrm{B}}^2/2m + V_0$. For $E_s < V_0$ the trigonometric functions $\cos[q_{\mathrm{B}}(z - nD - d_{\mathrm{A}})]$ and $\sin[q_{\mathrm{B}}(z - nD - d_{\mathrm{A}})]$ in equation (15) for the B layer should be replaced with the hyperbolic functions $\cosh[q_{\mathrm{B}}(z - nD - d_{\mathrm{A}})]$ and $\sinh[q_{\mathrm{B}}(z - nD - d_{\mathrm{A}})]$, respectively, with q_{B} defined by $E_s = -\hbar^2 q_{\mathrm{B}}^2/2m + V_0$. The coefficients $A_{j,s}^{(n+1)}$ and $B_{j,s}^{(n+1)}$ $(j = 1, 2)$ are determined successively by applying the transfer matrix t defined below, once the wavefunction $\phi_s(z)$ in the vacuum region $(z < 0)$ is specified.

These expressions for the electron wavefunctions for $z > 0$ should be compared with those in a perfect, periodic superlattice, which are written as (with $\lambda = (p_z, i)$) [15]

$$\phi_\lambda(z) = \sum_n \mathrm{e}^{\mathrm{i}np_zD}\{\Theta(z - nD)\Theta(nD + d_{\mathrm{A}} - z)\phi_{\mathrm{A},\lambda}^{(n+1)}(z) + \Theta(z - nD - d_{\mathrm{A}})\Theta[(n+1)D - z]\phi_{\mathrm{B},\lambda}^{(n+1)}(z)\}, \tag{16}$$

where

$$\phi_{\mathrm{A},\lambda}^{(n+1)}(z) = A_{1,\lambda}\cos[q_{\mathrm{A}}(z - nD)] + A_{2,\lambda}\sin[q_{\mathrm{A}}(z - nD)], \tag{17}$$

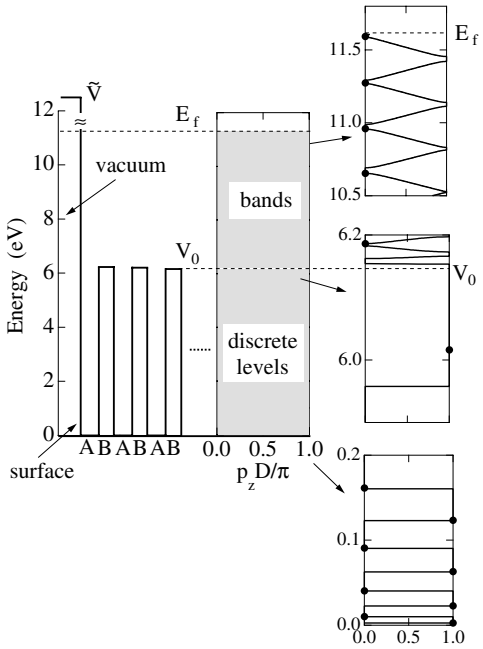

Figure 3. The energy diagrams of electrons in the semi-infinite Al/Ag superlattice (A = Al, B = Ag). Left-hand side: schematic energy diagram of the conduction band for electrons; the Fermi energy and potential height are $E_f = 11.63$ eV and $V_0 = 6.15$ eV, respectively, and the work function of aluminium is 4.25 eV; $\tilde{V} = 15.9$ eV is the potential height of the vacuum. Right-hand side: dispersion relation (energy versus p_z) of electrons in the infinite Kronig–Penney model with $d_A = d_{Al} = 121$ Å and $d_B = d_{Ag} = 97$ Å ($D = d_A + d_B = 218$ Å). The details of three energy regions near the bottom $E_\lambda = 0$, $E_\lambda = V_0$ and the top $E_\lambda = E_f$ are shown. Surface states in the semi-infinite superlattice are indicated by dots.

$$\phi_{B,\lambda}^{(n+1)}(z) = B_{1,\lambda}\cos[q_B(z - nD - d_A)] + B_{2,\lambda}\sin[q_B(z - nD - d_A)], \qquad (18)$$

with the coefficients $A_{j,\lambda}$ and $B_{j,\lambda}$ ($j = 1, 2$) determined from both the boundary conditions at the layer interfaces and the normalization conditions. The expressions for the electron wavefunctions in a perfect, periodic superlattice will be used in section 4.

In contrast, the wavefunction in the vacuum region $z < 0$ is simply written as

$$\phi_s(z) = \tilde{C}\exp(q_0 z), \qquad (19)$$

where q_0 is defined by $E_s = -\hbar^2 q_0^2/2m + \tilde{V}$; $\tilde{V}$ is the vacuum level measured from the bottom of the potential well of the A layer (see figure 3, below) and $\tilde{C}$ is a constant determined from the continuity of the wavefunction at the free surface and the normalization condition $\int_{-\infty}^{L} |\phi_s(z)|^2\,dz \simeq \int_0^L |\phi_s(z)|^2\,dz = 1$ for an extended electron eigenstate and $\int_{-\infty}^{\infty} |\phi_s(z)|^2\,dz \simeq \int_0^\infty |\phi_s(z)|^2\,dz = 1$ for a surface electron state.

Now we derive the equation determining the energies of the electrons. For this purpose we introduce a 2×2 transfer matrix t, whose elements are given by (with $\alpha = q_A d_A$ and $\beta = q_B d_B$) [15]

$$t_{11} = \cos\alpha\cos\beta - \frac{q_A}{q_B}\sin\alpha\sin\beta, \qquad (20)$$

$$t_{12} = q_A^{-1}\sin\alpha\cos\beta + q_B^{-1}\cos\alpha\sin\beta, \qquad (21)$$

$$t_{21} = -q_A\sin\alpha\cos\beta - q_B\cos\alpha\sin\beta, \qquad (22)$$

$$t_{22} = \cos\alpha\cos\beta - \frac{q_B}{q_A}\sin\alpha\sin\beta \tag{23}$$

for $E_s > V_0$ and

$$t_{11} = \cos\alpha\cosh\beta - \frac{q_A}{q_B}\sin\alpha\sinh\beta, \tag{24}$$

$$t_{12} = q_A^{-1}\sin\alpha\cosh\beta + q_B^{-1}\cos\alpha\sinh\beta, \tag{25}$$

$$t_{21} = -q_A\sin\alpha\cosh\beta + q_B\cos\alpha\sinh\beta, \tag{26}$$

$$t_{22} = \cos\alpha\cosh\beta + \frac{q_B}{q_A}\sin\alpha\sinh\beta \tag{27}$$

for $E_s < V_0$. With this transfer matrix t we write the electron wavefunction in the A layer and its derivative at the interface of the $(n+1)$th period as

$$\mathbf{\Phi}_{A,s}^{(n+1)}(nD) \equiv \begin{pmatrix} \tilde{\phi}_{A,s}^{(n+1)}(nD) \\ [\tilde{\phi}_{A,s}^{(n+1)}(nD)]' \end{pmatrix} = t^n \mathbf{\Phi}_{vac,s}(0), \tag{28}$$

where

$$\mathbf{\Phi}_{vac,s}(z) \equiv \tilde{C}\begin{pmatrix} \exp(q_0 z) \\ q_0\exp(q_0 z) \end{pmatrix}. \tag{29}$$

If we define the wavefunction $\mathbf{\Phi}_{B,s}^{(n+1)}$ in the B layer similarly to equation (28), its elements are determined from the continuity at the layer interfaces

$$\mathbf{\Phi}_{B,s}^{(n+1)}(nD + d_A) = \mathbf{\Phi}_{A,s}^{(n+1)}(nD + d_A). \tag{30}$$

The product t^n of the transfer matrix in equation (28) is calculated as

$$t^n = \begin{pmatrix} t_{11}S_n - S_{n-1} & t_{12}S_n \\ t_{21}S_n & t_{22}S_n - S_{n-1} \end{pmatrix}, \tag{31}$$

where

$$S_n = \frac{\varepsilon_2^n - \varepsilon_1^n}{\varepsilon_2 - \varepsilon_1} \tag{32}$$

and ε_1 and ε_2 $(=(\varepsilon_1)^{-1})$ are the eigenvalues of the unimodular transfer matrix t. For an electron within an energy band, $(\varepsilon_1, \varepsilon_2) = (e^{i\theta}, e^{-i\theta})$ with θ a real number defined by $\cos\theta = (t_{11} + t_{22})/2$ and

$$S_n = \frac{\sin n\theta}{\sin\theta}. \tag{33}$$

For a surface state the electron wavefunction should vanish for $z \to \infty$ or for $n \to \infty$. This condition together with equations (20)–(32) leads to

$$q_0 = \frac{\zeta - t_{11}}{t_{12}} = \frac{t_{21}}{\zeta - t_{22}}, \tag{34}$$

where $\zeta(|\zeta| < 1)$ is the eigenvalue (either ε_1 or ε_2) of the transfer matrix t with smaller modulus. The condition $|\zeta| < 1$ means that the surface states are found only inside the energy gap of the infinite Kronig–Penney system.

Thus the quantized electron fields in the semi-infinite superlattice can be written as

$$\Psi(\boldsymbol{x}) = \sum_{\Lambda} b_\Lambda \phi_s(z) e^{i\boldsymbol{p}_\parallel\cdot\boldsymbol{x}_\parallel}/\sqrt{S}, \tag{35}$$

where b_Λ and its Hermitian conjugate $b_\Lambda^\dagger$ are the annihilation and creation operators of electrons satisfying the anti-commutation relations $\{b_\Lambda, b_{\Lambda'}^\dagger\} = \delta_{\Lambda,\Lambda'}$ and $\{b_\Lambda, b_{\Lambda'}\} = 0$.

4. Electron–phonon interaction in superlattices

The deformation-potential coupling is assumed to be the mechanism of the electron–phonon interaction in metallic superlattices. In the Kronig–Penney model the calculated electron concentrations in the A and B layers coincide with those of bulk metals. This means that local charge neutrality holds in the layered structure and electrons are sensitive to the local lattice vibrations. Therefore the deformation-potential constants C_{A} and C_{B} of the bulk A and B metals are used for the electron–phonon coupling. The interaction of non-propagating surface phonons (with $\boldsymbol{k}_{\parallel} = 0$) with the electrons is described by the Hamiltonian

$$H_I = \sum_{\Lambda',\Lambda,J} \left(\frac{\hbar}{2\omega_J S}\right)^{1/2} b^{\dagger}_{\Lambda'} b_{\Lambda} (a_J + a^{\dagger}_{-J})\, \delta_{\boldsymbol{p}'_{\parallel},\boldsymbol{p}_{\parallel}} I_{\lambda'\lambda J}, \tag{36}$$

where the set of quantum numbers $\Lambda = (\boldsymbol{p}_{\parallel}, \lambda)$ specifies the complete electronic state and $J = \ell$.

Before considering the interaction of surface phonons with both the extended and surface states of electrons in semi-infinite superlattices, we first consider the interaction of surface phonons with bulk electrons in the perfect, periodic superlattice, thus neglecting the effect of the existence of a free surface for the electrons. This kind of approximation is often used in semi-infinite superlattices [11, 12, 22] because, as said above, the boundary conditions essentially affect the electron wavefunctions in a very small surface region provided that the size L of the system is large. Moreover, in this approach analytical calculations can be developed to some extent; hence, it is helpful in understanding the underlying physics associated with the surface phonon attenuation. In contrast, the full calculation of the surface phonon attenuation due to the interaction with the extended and surface electrons in the semi-infinite system is rather numerical in nature as we will see below.

For the interaction with the electrons in the perfect superlattices, the expression for $I_{\lambda'\lambda J}$ takes the form

$$I_{\lambda'\lambda J} = G(p'_z, p_z, J)\, F_{\lambda'\lambda J}, \tag{37}$$

where

$$F_{\lambda'\lambda J} = \frac{C_{\mathrm{A}}}{\rho_{\mathrm{A}}^{1/2}} \int_0^{d_{\mathrm{A}}} \mathrm{d}z\, \phi^*_{\mathrm{A},\lambda'}(z) \frac{\mathrm{d}U_{\mathrm{A},J}(z)}{\mathrm{d}z} \phi_{\mathrm{A},\lambda}(z) + \frac{C_{\mathrm{B}}}{\rho_{\mathrm{B}}^{1/2}} \int_0^{d_{\mathrm{B}}} \mathrm{d}z\, \phi^*_{\mathrm{B},\lambda'}(z) \frac{\mathrm{d}U_{\mathrm{B},J}(z)}{\mathrm{d}z} \phi_{\mathrm{B},\lambda}(z), \tag{38}$$

with $\phi_{\mathrm{A},\lambda}(z) = \phi^{(1)}_{\mathrm{A},\lambda}(z)$, $\phi_{\mathrm{B},\lambda}(z) = \phi^{(1)}_{\mathrm{B},\lambda}(z + d_{\mathrm{A}})$ (see equations (17) and (18)), $U_{\mathrm{A},J}(z) = U^{(1)}_{\mathrm{A},J}(z)$ and $U_{\mathrm{B},J}(z) = U^{(1)}_{\mathrm{B},J}(z + d_{\mathrm{A}})$, is the overlapping integral of the electron and phonon wavefunctions over a unit period, and

$$G(p'_z, p_z, J) = G(p'_z, p_z, \ell) = \frac{1}{1 - \mathrm{e}^{\mathrm{i}(p_z - p'_z)D}(T_\ell)_{11}}. \tag{39}$$

Here we remark that for the bulk phonon interaction with the electrons in an assumed perfect superlattice $G(p'_z, p_z, J)$ becomes a function representing the conservation of superlattice wavenumbers [15], i.e.,

$$G(p'_z, p_z, J) = G(p'_z, p_z, k_z) = N\Delta(p'_z - p_z - k_z), \tag{40}$$

where N is the number of periodicity, $\Delta(p_z) = 1$ if p_z is a reciprocal superlattice number and $\Delta(p_z) = 0$ otherwise.

On the other hand, for the interaction with electrons in the semi-infinite superlattices the expression for $I_{\lambda'\lambda J}$ is

$$I_{\lambda'\lambda J} = \sum_{n=0}^{\infty}\left\{ \frac{C_{\rm A}}{\rho_{\rm A}^{1/2}} \int_{nD}^{nD+d_{\rm A}} {\rm d}z\, [\tilde{\phi}^{(n+1)}_{{\rm A},\lambda'}(z)]^* \frac{{\rm d}\tilde{U}^{(n+1)}_{{\rm A},J}(z)}{{\rm d}z} \tilde{\phi}^{(n+1)}_{{\rm A},\lambda}(z) \right.$$
$$\left. + \frac{C_{\rm B}}{\rho_{\rm B}^{1/2}} \int_{nD+d_{\rm A}}^{(n+1)D} {\rm d}z\, [\tilde{\phi}^{(n+1)}_{{\rm B},\lambda'}(z)]^* \frac{{\rm d}\tilde{U}^{(n+1)}_{{\rm B},J}(z)}{{\rm d}z} \tilde{\phi}^{(n+1)}_{{\rm B},\lambda}(z) \right\}, \tag{41}$$

with $\tilde{U}^{(n+1)}_{{\rm A(B)},J} = [(T_\ell)_{11}]^n U^{(n+1)}_{{\rm A(B)},J}$. The integrations of equation (41) cannot be done analytically but there exists an analytical expression (though lengthy) for $F_{\lambda'\lambda J}$ defined by equation (38) [15].

5. Attenuation rates of surface phonons

Just like the case for the bulk metals [23, 24] the interaction between electrons and phonons is assumed to be weak enough for their respective states to be relatively long lived so that the first order perturbation theory can be used to calculate the scattering rate. Thus, applying the Fermi golden rule for the transition rate, we can derive the equation governing the time evolution for the deviation Δn_J of phonon occupation number n_J from the thermal equilibrium value:

$$-\frac{\Delta \dot{n}_J}{\Delta n_J} = \tau_J^{-1} = \frac{2\pi}{\omega_J S} \sum_{\Lambda',\Lambda} |I_{\lambda'\lambda J}|^2 (f_\Lambda - f_{\Lambda'}) \delta_{\boldsymbol{p}'_\parallel,\boldsymbol{p}_\parallel} \delta(E_{\Lambda'} - E_\Lambda - \hbar\omega_J), \tag{42}$$

where τ_J is the relaxation time of the surface phonon specified by J and f_Λ is the electron occupation number.

According to our previous remark in section 4, we first consider the attenuation of surface phonons due to the interaction with *the electrons in a perfect, periodic superlattice*. The wavenumber k_z of the surface phonons is complex and the conservation of the superlattice wavenumbers does not hold. In this case equation (39) leads to the form factor which depends on the transfer of the superlattice wavenumber of electrons to the surface phonon with $\omega = \omega_\ell$,

$$|G(p'_z, p_z, \ell)|^2 = \frac{1}{1 - 2(T_\ell)_{11}\cos[(p'_z - p_z)D] + [(T_\ell)_{11}]^2}. \tag{43}$$

This expression means that the electrons with a wavenumber p_z in a continuous range can interact with surface phonons (see figure 4 below for a numerical example). However, the energy conservation still has to be satisfied. Here we note that for $(T_\ell)_{11} < 0\ (>0)|G(p'_z, p_z, \ell)|^2$ has peaks at $(p'_z - p_z)D/\pi = \pm 1, \pm 3, \ldots\ (=0, \pm 2, \ldots)$ corresponding to the wavenumber-conserving emission and absorption of a zone-boundary (zone-centre) surface phonon by electrons. The attenuation rate now becomes

$$\tau_J^{-1} = \frac{L^2}{(2\pi)^2}\frac{m}{\hbar} \sum_i \sum_n \int_{-\pi/D}^{\pi/D} {\rm d}p_z \frac{|F_{\lambda'\lambda J}|^2}{1 - 2(T_\ell)_{11}\cos[(p'_z - p_z)D] + [(T_\ell)_{11}]^2} \left| \frac{{\rm d}E_{p'_z,i'}}{{\rm d}p'_z} \right|^{-1}_{p'_z = p^{(n)}}, \tag{44}$$

with $J = \ell, \lambda = (p_z, i), \lambda' = (p'_z, i')$ and $E_{p'_z,i'} = E_{p_z,i} + \hbar\omega_\ell$. The integration with respect to p_z should be carried out over the region in the mini-Brillouin zone where the real wavenumber p'_z satisfying the energy conservation $E_{p'_z,i'} = E_{p_z,i} + \hbar\omega_\ell$ may be found. In such cases there exist, in general, two solutions $p'_z = p^{(1)}$ and $p^{(2)}$ with $p^{(1)} = -p^{(2)}$ for a given p_z. Hence, the sum over n in equation (44) is taken over $n = 1$ and 2.

Next we study the attenuation due to the interaction with *both the extended and surface states of electrons in a semi-infinite superlattice*. For a superlattice with $D \sim 100$ Å and in the approximation that the level broadening of the electron energies is neglected, the transitions between the electronic states by the emission and/or absorption of a sub-THz surface phonon

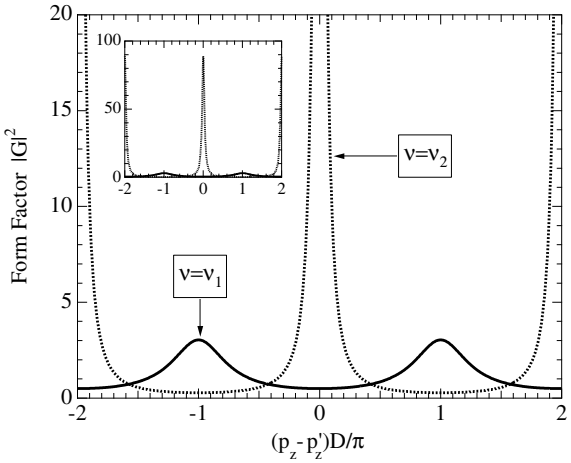

Figure 4. Form factor $|G|^2$ versus wavenumber transfer $(p_z - p'_z)$ to the low-frequency surface phonons at ν_1 (the zone-boundary mode, solid curve) and at ν_2 (the zone-centre mode, dotted curve) in the Al/Ag superlattice. The assumed parameters are the same as for figures 1 and 3.

are prohibited for $\lambda = s$ and $\lambda' = s'$ with E_s, $E_{s'} < V_0$. Thus, for the attenuation of a surface phonon with $J = l$, we may consider the scattering processes where (a) both $\lambda = s$ and $\lambda' = s'$ in equation (41) correspond to the extended electron states and (b) $\lambda = s$ corresponds to the surface state and $\lambda' = s'$ to the extended state, and vice versa. The attenuation rate due to these processes (a) and (b) is written as

$$\tau_J^{-1} = \tau_{J,(a)}^{-1} + \tau_{J,(b)}^{-1}, \tag{45}$$

where

$$\tau_{J,(a)}^{-1} = \frac{m}{\hbar} \int \mathrm{d}E_s \, \tilde{D}(E_s)\tilde{D}(E_s + \hbar\omega_J)|I_{s'sJ}|^2_{E_{s'}=E_s+\hbar\omega_J}, \tag{46}$$

$$\tau_{J,(b)}^{-1} = \frac{m}{\hbar} \sum_s \{\tilde{D}(E_s + \hbar\omega_J)|I_{s'sJ}|^2_{E_{s'}=E_s+\hbar\omega_J} + \tilde{D}(E_s - \hbar\omega_J)|I_{ss'J}|^2_{E_{s'}=E_s-\hbar\omega_J}\}, \tag{47}$$

$\tilde{D}(E)$ is the density of states of the extended electrons in the semi-infinite Kronig–Penney system and the sum over s in equation (47) is taken only over surface states of electrons.

It should be noted here that, for the extended electronic states in the semi-infinite Kronig–Penney model, we can use the same density of states as the one in the infinite Kronig–Penney model. This is assured by the general theory of eigenvalues that the energy spectrum is not significantly affected by the chosen boundary condition, provided that the system size L is large [21]. More precisely, a fraction of L^{-1} of energies enter and leave any energy interval when we change from one boundary condition to the other, and this is negligible in the limit of large L. Thus the energy spectra are essentially the same for the infinite and semi-infinite superlattice systems, though the electron wavefunctions are quite different even if the energies are the same. So, it is important to take account of the modification of the wavefunctions due to the introduction of a surface. For instance, the local density of states of electrons near the surface region should be different from those inside the superlattice. These effects have been considered properly in the calculation of equations (46) and (47).

Table 1. Frequencies (ν) and decay constants (T_{11}) of the sub-THz localized surface vibrations in the Al/Ag superlattice with $d_A = d_{Al} = 121$ Å and $d_B = d_{Ag} = 97$ Å ($D = d_A + d_B = 218$ Å).

ℓ	ν_ℓ (GHz)	$(T_\ell)_{11}$
1	122	−0.426
2	221	0.894
3	362	−0.548
4	448	0.662

6. Numerical calculations

The attenuation rates of the extended and surface phonons in an Al/Ag superlattice with $d_A = d_{Al} = 121$ Å and $d_B = d_{Ag} = 97$ Å ($D = 218$ Å) are calculated from the above equations. These layer thicknesses are the same as those of the superlattice used for the picosecond ultrasound experiment by Chen *et al* [12]. We also assume other parameters used by Chen *et al* to analyse phonon properties in Al/Ag superlattices: $\rho_A = \rho_{Al} = 2.7$ g cm^{-3}, $\rho_B = \rho_{Ag} = 10.5$ g cm^{-3}, $v_A = v_{Al} = 6.4 \times 10^5$ cm s^{-1} and $v_B = v_{Ag} = 4.0 \times 10^5$ cm s^{-1}. The Fermi energies of electrons in aluminium and silver are 11.63 and 5.48 eV, respectively. The potential barrier height V_0 deduced from the Fermi energies is therefore $V_0 = 6.15$ eV. From the Fermi energies of aluminium and silver, we also find the deformation-potential constants $C_A = C_{Al} = -7.57$ eV and $C_B = C_{Ag} = -3.65$ eV.

6.1. Frequencies and lattice displacements for surface phonons

The dots in figure 1 show the frequencies of the non-propagating surface modes that exist in the semi-infinite superlattice with an Al (A) layer at the free surface $z = 0$. They appear either at band edges or in forbidden bands between the solid curves representing the dispersion relation of the longitudinal phonons propagating along the growth direction of the Al/Ag superlattice. These eigenfrequencies have been previously calculated by Chen *et al* [12] and the corresponding decay coefficients $(T_\ell)_{11}$ are tabulated in table 1 for the lowest four frequencies. As expected, the magnitude of the decay coefficient $|(T_\ell)_{11}|$ is close to unity at a frequency near the band edge (ν_2, for instance), suggesting the slow decay of the displacement amplitude.

In figure 2 we show the lattice displacement $W_J(z)$ ($J = \ell$) versus the distance away from the surface for the lowest two eigenfrequencies ν_1 and ν_2; the phase has been chosen so that $W_J(z)$ is real. The decay of the displacement amplitude at ν_2 is very slow compared to the displacement amplitude at ν_1. It exhibits a bulklike oscillatory behaviour.

Figure 3 shows the dispersion relation of electrons calculated from the semi-infinite Kronig–Penney model together with a schematic energy profile for the electrons. Because of the large thickness ($d_B = d_{Ag} = 97$ Å) of the potential barrier (silver layer) for electrons, the band widths are negligibly small at energies below V_0, leading to discrete energy levels for $E_s < V_0$. Energy bands of a sizeable width are found only for $E_s > V_0$. In the superlattice considered, no interband transition is allowed for electrons by the absorption or emission of a sub-THz phonon.

6.2. Attenuation rate of surface phonons

Figure 4 displays the form factor $|G|^2$ versus wavenumber transfer $p_z - p'_z$ to a surface phonon from electrons assumed to belong to a perfect, periodic superlattice (an infinite Kronig–Penney

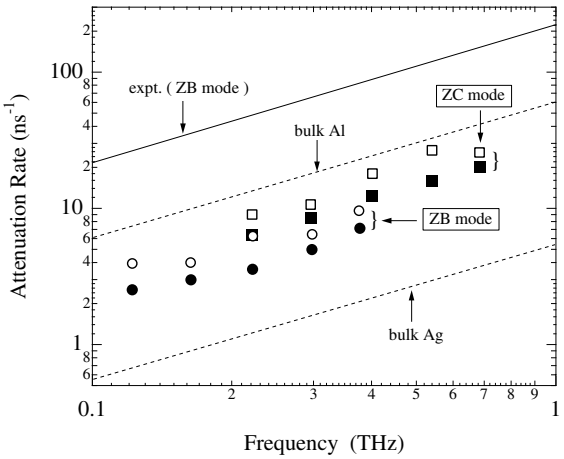

Figure 5. The attenuation rates versus frequency for the surface phonons (the lowest zone-boundary (ZB, circles) and zone-centre (ZC, squares) modes) localized at the truncated surface with an Al first layer and for various spatial periods (bilayer thicknesses) $D = 218$, 163, 120, 89.3 and 70.4 Å of the superlattice and a constant ratio (=0.8) of the Ag-to-Al thickness. The results due to the interaction with the electrons in the semi-infinite (in the perfect, periodic) superlattice are shown by filled (open) circles and squares. The solid line is the least-squares fit to the experimental damping rates of the ZB mode (from [12]). The dotted lines show the attenuation rates in the bulk aluminium and silver calculated from the Pippard formula.

model). For a surface mode which penetrates deep into the superlattice with $|(T_\ell)_{11}| \simeq 1$ (the zone-centre surface phonon at $\nu = \nu_2$), the form factor has large peaks like δ-functions expected for the interaction of bulk phonons. However, for the interaction of the zone-boundary surface phonon (at $\nu = \nu_1$) well localized near the surface of the superlattice ($|(T_\ell)_{11}| < 1$), small and broad humps are found, suggesting the relaxation of the wavenumber conservation along the layer interfaces.

In the calculation of the attenuation rate we have considered, in addition to the superlattice with $D = 218$ Å, four kinds of Al/Ag superlattice with bilayer thicknesses $D = 163$, 120, 89.3 and 70.4 Å, which are used in the experimental measurements of the damping [12]. In these superlattices the ratio of the Ag-to-Al thickness is 0.8. The attenuation rates plotted in figure 5 are those obtained for the lowest zone-boundary (ZB, circles) and zone-centre (ZC, squares) surface phonons.

We see in figure 5 that the calculated attenuation rates roughly exhibit a linear dependence on frequency as observed experimentally, though there exist some fluctuations arising from the changes of the electron band structure sensitive to the thickness of the constituent layers. However, the magnitudes calculated with the electronic states both in the perfect, periodic (open symbols) and semi-infinite (filled symbols) systems are much smaller than the experiments. For the ZB mode (circles) the theoretical attenuation rates are about a factor of ten smaller than the experimental damping rates shown by the solid line exhibiting a least-squares fit to the ZB mode data (from [12]), though the former are of the same order of magnitude as calculated from the Pippard theory for bulk phonons [14].

For the ZC mode (squares), the theoretical attenuation rate is larger than that for the ZB mode. An accurate experimental measurement for the ZC mode was made only at a single frequency (480 GHz) and the damping of this mode is reported to be about a factor of two higher than would be expected on the basis of an extrapolation of the low-frequency data for the ZB mode [12]. But the calculated attenuation is again about a factor of ten smaller than these data.

Thus, the inclusion of the effects of the surface on the electronic states in the superlattice does not help to increase the agreement with the experimental results. We note that in this calculation the dominant contribution to the attenuation rate equation (45) comes from the processes where both the initial and final electrons are in the extended states, i.e., $\tau^{-1}_{J,(a)}$ equation (46). We also remark here that similarly to the case for the bulk phonons the attenuation of surface phonons is predicted to occur predominantly in the Ag layers, though they have smaller thickness and smaller deformation-potential constant [15].

7. Conclusions

We have extended the Pippard theory of the electron–phonon interaction in a bulk metal to multilayered structures in order to explain the damping of surface phonons in Al/Ag superlattices measured by Chen *et al* [12]. The calculated attenuation rate assuming the interaction with electrons in both infinite and semi-infinite periodic superlattices roughly exhibits a linear frequency dependence just as in the experiments. However, the absolute magnitude is much smaller than the measured damping rates; that is, the results of the Pippard theory applied to the superlattice do not agree with the experimental data. Thus we conclude that the extension of the Pippard theory simply taking account of the folded band structures of both electrons and phonons in the mini-Brillouin zone of a superlattice cannot explain the large damping of the high-frequency surface phonons in Al/Ag superlattices.

In semiconductor confined structures the existence of the ripple mechanism for the electron–phonon interaction has been suggested in addition to the deformation-potential and piezoelectric couplings [25, 26]. This interaction originates from the time modulation of the electron quantization energies caused by the heterointerface vibrations associated with acoustic phonons. However, in our formulation of the electron–phonon interaction in metallic superlattices we have not considered this effect on the phonon attenuation in metallic superlattices. This is partly because we want to estimate the correction to the Pippard theory for the phonon attenuation in superlattices due to the deformation-potential coupling. Also it is doubtful whether this effect is really large for the superlattice with a large bilayer thickness $D \simeq 100$ Å.

Another contribution to be studied further would be the effect of broadening of the electronic energy states due to the scattering of electrons. This effect makes it possible for the surface and extended states of electrons to absorb or emit surface phonons via interband or interlevel transitions and hence will contribute to enhancing the attenuation of surface phonons.

To conclude, our results suggest that a more elaborated theory of electron–phonon interaction or a calculation based on other mechanisms beyond the one developed in the present work will be needed to resolve the attenuations of surface phonons observed in metallic superlattices.

Acknowledgments

One of the authors (ST) acknowledges University Pierre et Marie Curie (Paris VI) and Ecole Normale Superieure for hospitality. This work was supported in part by the University Pierre et Marie Curie and by a Grant-in-Aid for Scientific Research from the Ministry of Education, Science and Culture of Japan (grant No 12640304).

References

[1] Lord Rayleigh 1887 *Proc. Lond. Math. Soc.* **17** 4
[2] Camley R E, Djafari-Rouhani B, Dobrzynski L and Maradudin A A 1983 *Phys. Rev.* B **27** 7318

[3] Sapriel J, Djafari-Rouhani B and Dobrzynski L 1983 *Surf. Sci.* **126** 197
[4] Djafari-Rouhani B, Dobrzynski L, Duparc O H, Camley R E and Maradudin A A 1983 *Phys. Rev.* B **28** 1711
[5] Dobrzynski L, Djafari-Rouhani B and Duparc O H 1984 *Phys. Rev.* B **29** 3138
[6] Mizuno S and Tamura S 1996 *Phys. Rev.* B **53** 4549
[7] Aono T and Tamura S 1998 *Phys. Rev.* B **58** 4838–45
[8] Tanaka Y and Tamura S 1998 *Phys. Rev.* B **58** 7958–65
[9] Colvard C, Merlin R, Klein M V and Gossard A C 1980 *Phys. Rev. Lett.* **45** 298
Colvard C, Gant T A, Klein M V, Merlin R, Fischer R, Morkoc H and Gossard A C 1985 *Phys. Rev.* B **31** 2080
Jusserand B, Paquet D and Regreny A 1984 *Phys. Rev.* B **30** 6245
[10] Tamura S, Hurley D C and Wolfe J P 1988 *Phys. Rev.* B **38** 1427
Tamura S 1988 *Phys. Rev.* B **39** 1261
[11] Grahn H T, Maris H J, Tauc J and Abeles B 1988 *Phys. Rev.* B **38** 6066
[12] Chen W, Lu Y, Maris H J and Xiao G 1994 *Phys. Rev.* B **50** 14506
[13] Perrin B, Bonello B, Jeannet J-C and Romatet E 1996 *Physica* B **219/220** 681
[14] Pippard A B 1960 *Proc. R. Soc.* A **257** 165
See, also
Tucker J W and Rampton V W 1972 *Microwave Ultrasonics in Solid State Physics* (Amsterdam: North-Holland)
Hepfer K C and Rayne A 1971 *Phys. Rev.* B **4** 1050
[15] Tamura S and Perrin N 2002 *J. Phys.: Condens. Matter* **14** 689 and references therein
[16] Mizuno S and Tamura S 1992 *Phys. Rev.* B **45** 734
[17] Ashcroft N W and Mermin N D 1976 *Solid State Physics* (New York: Saunders) ch 18
[18] Djafari-Rouhani B, Dobrzynski L and Masri P 1985 *Phys. Rev.* B **31** 7739
[19] Bloss W L 1991 *Phys. Rev.* B **44** 8035
[20] Tikhodeev S G 1991 *Solid State Commun.* **78** 339
[21] Ledermann W 1944 *Proc. R. Soc.* A **182** 362
See, also,
Maradudin A A, Montroll E W, Weiss G H and Ipatova I P 1971 *Solid State Physics* vol 3 (New York: Academic)
[22] Maradudin A A and Mills D L 1968 *Phys. Rev.* **173** 881
[23] Ivchenko E L and Pikus G E 1997 *Superlattices and Other Heterostructures* 2nd edn (New York: Springer) ch 3
[24] For a review see
Ridley B K 1997 *Electrons and Phonons in Semiconductor Multilayers* (Cambridge: Cambridge University Press)
[25] Vasko F T and Mitin V V 1995 *Phys. Rev.* B **52** 1500
[26] Knipp P A and Reinecke T L 1995 *Phys. Rev.* B **52** 5923